Pergamon

Int. J. Multiphase Flow Vol. 23, No. 6, pp. 1063–1083, 1997

Printed in Great Britain

PII: S0301-9322(97)00027-X

0301-9322/97 $17.00 + 0.00

HYDRODYNAMIC CHARACTERISTICS OF COUNTER-CURRENT TWO-PHASE FLOW IN VERTICAL AND INCLINED CHANNELS: EFFECTS OF LIQUID PROPERTIES

S. M. GHIAASIAAN, X. WU, D. L. SADOWSKI and S. I. ABDEL-KHALIK

G. W. Woodruff School of Mechanical Engineering, Georgia Institute of Technology, Atlanta, GA 30332-0405, U.S.A.

(Received 24 June 1996; in revised form 4 April 1997)

Abstract—Flow patterns, counter-current flow limitation (flooding), and gas hold-up (void fraction) in counter-current flow in vertical and inclined channels were experimentally investigated. Tests were performed in a 2 m-long channel with 1.9 cm inner diameter, using air, and demineralized water, mineral and paraffinic oils, covering a surface tension range of 0.0128–0.072 N/m, and a liquid viscosity range of 1×10^{-3}–1.85×10^{-1} Ns/m^2. The liquid and gas superficial velocity ranges for the tests with demineralized water were $0 \leqslant U_{LS} \leqslant 54$ cm/s and $1 \leqslant U_{GS} \leqslant 299$ cm/s, for tests with mineral oil were $0 \leqslant U_{LS} \leqslant 23$ cm/s and $1 \leqslant U_{GS} \leqslant 248$ cm/s, and for paraffinic oil were $0.15 \leqslant U_{LS} \leqslant 11.6$ cm/s and $1 \leqslant U_{GS} \leqslant 224$ cm/s, respectively. The examined channel angles of inclination with respect to the vertical line were 0, 30 and 68°.

Flooding data were significantly different from pure water results only at very high liquid viscosities. The effect of liquid viscosity on gas hold-up and flow patterns was significant, furthermore, and several existing models and correlations were unable to correctly predict the data trends. With increasing the liquid viscosity the parameter range of the slug flow pattern expanded for all angles of inclination, and froth flow replaced the churn flow pattern in the vertical configuration and it replaced the churn/stratified and semi-stratified patterns in inclined configurations. The churn–stratified flow pattern is predominantly wavy stratified and is interrupted by upward-moving flooding-type waves. Semi-stratified is a periodic pattern where in each period the flow regime is initially wavy stratified while liquid accumulates in the bottom portion of the test section and forms a large liquid slug which subsequently moves upwards in the channel. © 1997 Elsevier Science Ltd.

Key Words: two-phase flow, counter-current flow, inclined channels, flow patterns, void fraction, flooding

1. INTRODUCTION

Powerful computer codes, based on the numerical solution of separated-flow two- and three-fluid conservation equations, and equipped with robust numerical solution algorithms, are now available for the analysis of multiphase systems (Carlson *et al.* 1990; Passamehmetoglu *et al.* 1990; Amarasooriya and Theofanous 1988; Ren *et al.* 1994). Solution of multi-fluid conservation equations is only possible when constitutive relations, including relations representing the inter-fluids transfer processes, are provided. The predictions made by the multi-fluid codes can thus be reliable only when their constitutive relations adequately approximate the modeled physical processes. Flow patterns, their hydrodynamic characteristics, and their transition conditions, are among the most important constitutive relations. An understanding of the flow patterns, in addition to providing for the representation of the morphology of the flow field, is crucial in modeling the various interphase transfer processes. The objective of this investigation was to experimentally study the hydrodynamic aspects of counter-current two-phase flow in vertical and inclined channels, addressing the two-phase flow patterns, gas hold-up, and the counter-current flow limitation (CCFL), or flooding. A brief review of the relevant literature is provided below.

Counter-current two phase flow is a common occurrence in hypothetical nuclear reactor accidents, and is encountered in chemical and petrochemical systems, e.g. in the operation of some bubble columns with liquid through-flow. Despite extensive literature dealing with various aspects

of flow patterns in two-phase flow, except for the counter-current flow limitation (CCFL) phenomenon, or flooding, little research addressing hydrodynamic and transport phenomena in counter-current channel flow has been reported.

Published studies dealing with flow patterns in counter-current flow are few. Yamaguchi and Yamazaki (1982, 1984) performed experiments in vertical channels with 4 and 8 cm inner diameters, and identified four major flow regimes: bubbly, which could be maintained only at very low superficial gas velocities; slug, which occupied an extensive portion of the entire flow map; semi-annular, which represented the transition between slug and annular regimes; and annular. Ghiaasiaan *et al.* (1995a) recently performed experiments with air and water, using vertical and inclined channels. They studied the counter-current flow patterns, and measured the channel average gas hold-ups using quick-action valves. The flow patterns, which were relatively sensitive to the channel angle of inclination, included some flow patterns which may not occur in cocurrent flow. Models and correlations applicable to flow regime transitions in counter-current flow are few, and include the following.

Taitel and Barnea (1983) proposed a mechanistic set of models for flow regime transitions, by dividing the entire flow map into three major patterns: bubbly, slug, and annular. According to their model, bubbly flow can exist when the following conditions are met

$$U_{LS} \leqslant U_{GS} + U_B - (4U_{GS}U_B)^{1/2} \quad [1]$$

$$0.3U_{LS} + 0.7U_{GS} < 0.21U_{GS} \quad [2]$$

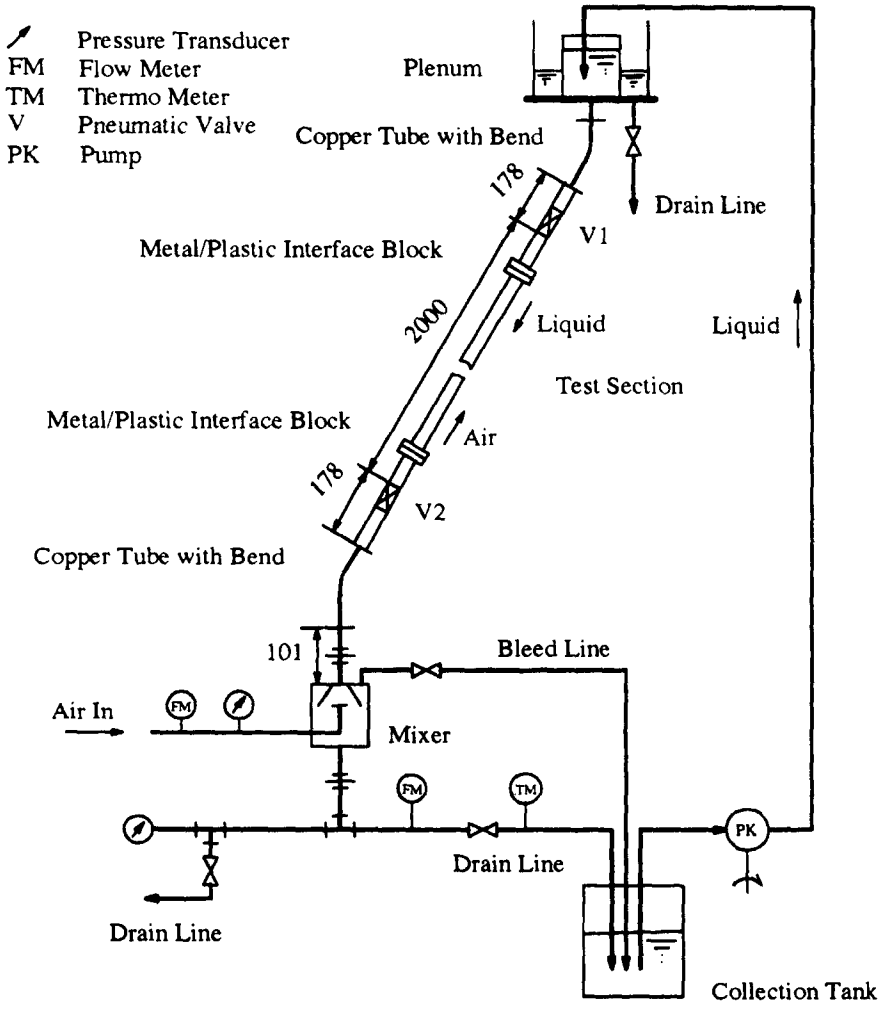

Figure 1. Schematic of the test facility (all dimensions in mm).

where U_{LS} and U_{GS} are the liquid and gas superficial velocities, and the rise velocity of large bubbles, U_B, is found from (Harmathy 1960)

$$U_B = 1.53\left[\frac{\sigma g \Delta\rho}{\rho_L^2}\right]^{1/4}, \qquad [3]$$

where σ is the surface tension, g is the gravitational acceleration, and $\Delta\rho = \rho_L - \rho_G$ with ρ_L and ρ_G representing the liquid and gas densities. Note that everywhere in this paper U_{LS} is positive when it is downwards, and U_{GS} is positive when it is upwards. Equations [1] and [2], with equal signs, represent boundaries b and c, respectively, in Taitel and Barnea's flow regime map.

In addition to the above models, Taitel and Barnea (1983) also proposed a model for the slug-to-annular flow regime transition (boundary d), and a model representing the conditions sufficient for the development of annular flow (boundary e). The latter models, however, did not agree with the experimental data of Ghiaasiaan *et al.* (1995). Boundary e, in particular, approximately coincides with Wallis's flooding correlation (Wallis 1969).

The slug-to-churn flow transition in vertical, cocurrent channel flow has been modeled by several investigators. These models, as long as their basic derivation is not limited to cocurrent flow, may be applied to counter-current flow. McQuillan and Whalley (1985) proposed a model essentially identical to the aforementioned boundary e of Taitel and Barnea (1983). A model, for slug-to-churn flow regime transition, proposed by Mishima and Ishii (1984), can be represented as

$$\alpha \geqslant 1 - 0.813\left\{\frac{(C_0 - 1)U_m + 0.35(g\Delta\rho D/\rho_L)^{1/2}}{U_m + 0.75(g\Delta\rho D/\rho_L)^{0.5}(g\Delta\rho D^3/\rho_L \nu_L^2)^{1/18}}\right\}^{0.75} \qquad [4]$$

where C_0 is the two-phase drift flux distribution coefficient (Wallis 1969), D represents the channel diameter, ν_L represents the liquid kinematic viscosity, and U_m is the two-phase volumetric flux.

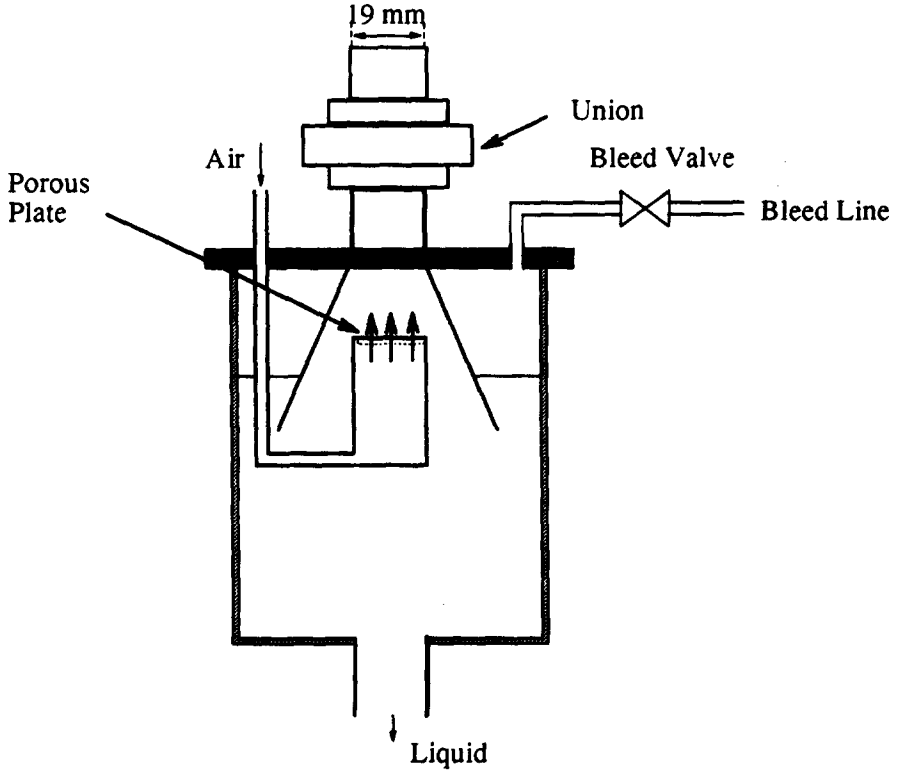

Figure 2. Schematic of the mixer.

The right-hand side of [4] represents the mean gas hold-up in the Taylor bubbles, and α, the channel mean gas hold-up, is found using the drift flux model

$$\alpha = \frac{U_{GS}}{C_0 U_m + V_{Gj}} \quad [5]$$

where, for cocurrent upward flow

$$C_0 = 1.2 - 0.2(\rho_G/\rho_L)^{0.5} \quad \text{for round tubes} \quad [6]$$

$$C_0 = 1.35 - 0.35(\rho_G/\rho_L)^{0.5} \quad \text{for rectangular ducts.} \quad [7]$$

The gas drift velocity, V_{Gj}, is found from

$$V_{Gj} = U_{B,\infty} = 0.35(g\Delta\rho D/\rho_L)^{1/2}. \quad [8]$$

The two-phase mixture volumetric flux, U_m, is defined as

$$U_m = U_{GS} - U_{LS}. \quad [9]$$

For cocurrent downward flow, and for the case of slug flow with $U_m < 0$ (downward mixture volumetric flux) and ascending Taylor bubbles $C_0 \lesssim 1$ may be more appropriate, as noted by Martin (1976) in his experiments with air and water. For cocurrent downward flow Martin obtained $C_0 = 0.93$, 0.90 and 0.86 for channel diameters of 2.6, 10.16 and 14 cm, respectively.

Jayanti and Hewitt (1992) recently reviewed the slug to churn regime transition models of McQuillan and Whalley (1985) and Mishima and Ishii (1984), and a model proposed by Brauner and Barnea (1985). Jayanti and Hewitt indicated that the model of Mishima and Ishii, although problematic in its implied basic assumptions regarding the void fraction in liquid slugs (which can result in the prediction of unphysically high void fractions in the liquid slugs), agreed

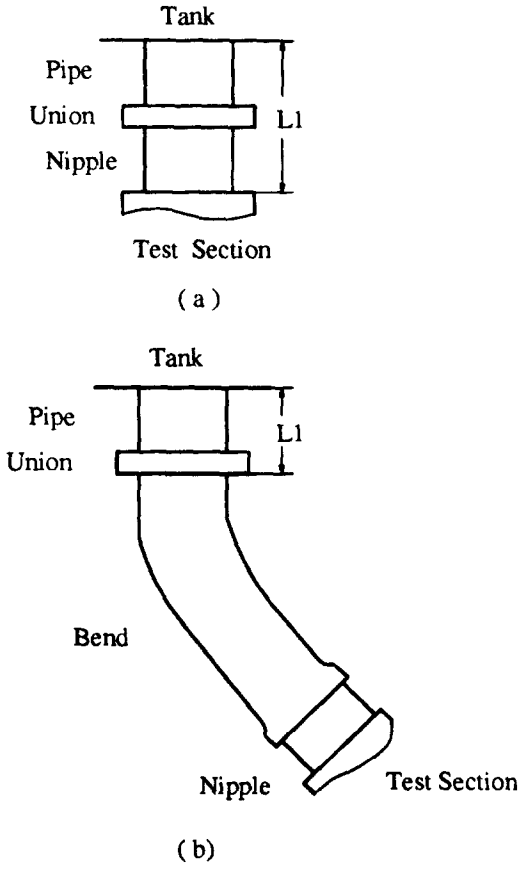

Figure 3. Configuration of the fittings. (a) Vertical test section. (b) Inclined test section.

well with experimental data at low liquid flow rates. The model of Mishima and Ishii (1984) is thus considered here as an empirical correlation.

Usui (1989) derived the following correlation (originally for cocurrent downward flow) for the slug-to-annular regime transition, by intersecting the gas hold-up relations for the two flow patterns

$$\frac{C_1}{C_0 \mathrm{Fr}_L} - \{[C_0 - (2C_w \mathrm{Fr}_L^2)^{7/23} C_0]^{-1} - 1\} \frac{U_{GS}}{U_{LS}} = 1, \quad [10]$$

where C_w represents the wall Fanning friction factor, and the liquid Freude number, Fr_L is defined as

$$\mathrm{Fr}_L = U_{LS}(gD\Delta\rho/\rho_L)^{-1/2}. \quad [11]$$

The two-phase distribution coefficient, and the Eotvos number, E_0, are found from

$$C_0 = 1.2 - (2.95 + 350E_0^{-1.3})^{-1} \quad [12]$$

$$E_0 = g\Delta\rho D^2/\sigma. \quad [13]$$

Parameter C_1 in [10] is the dimensionless coefficient of the following correlation for the rise velocity of Taylor bubbles (Wallis 1969)

$$U_{B,\infty} = C_1(g\Delta\rho D/\rho_L)^{1/2}, \quad [14]$$

where

$$C_1 = 0.345\{1 - \exp[(3.37 - E_0)/10]\}. \quad [15]$$

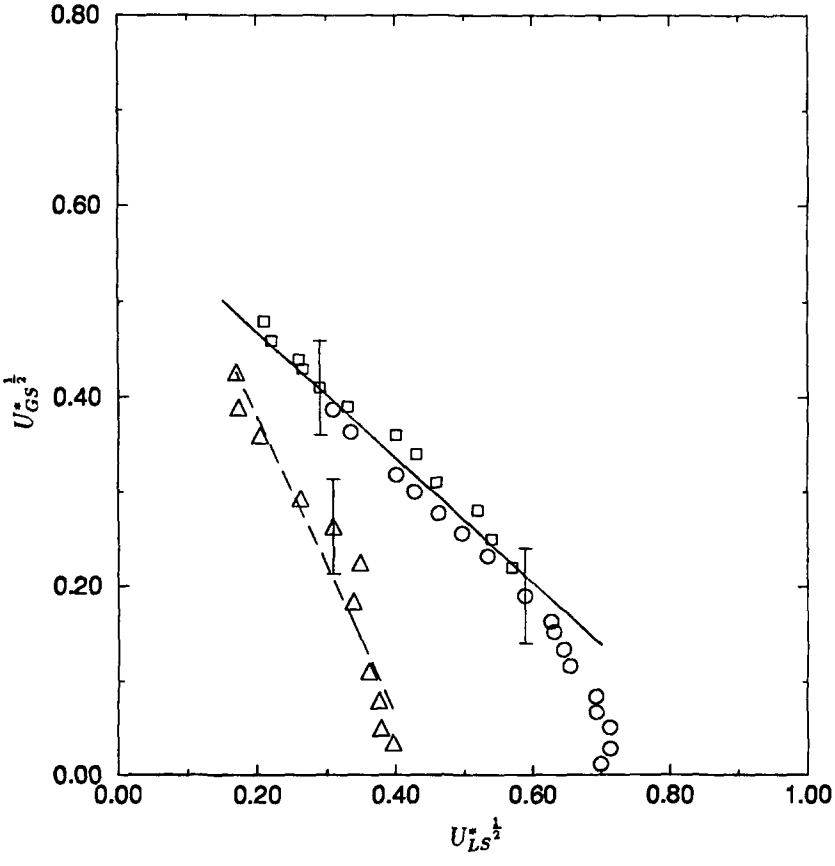

Figure 4. Flooding data for the vertical test section: □, water; ○, mineral oil; △, paraffinic oil; —, flooding line [16], $m = 0.66$, $C = 0.6$; – – –, flooding line [16], $m = 1.567$, $C = 0.692$.

2. EXPERIMENTS

2.1. Apparatus

The test apparatus used in this investigation is schematically shown in figure 1, and includes a liquid-filled plenum enclosed in a large open tank at the top, a transparent tubular test section, and a sealed mixer tank at the bottom.

The plenum in the tank at the top is a 28-cm long cylinder with 20 cm i.d., and is enclosed in a transparent parallelepiped box, open at the top, with a 30 × 30 cm base and 41 cm in height. Liquid is pumped into the upper plenum to maintain it overflowing during the experiments.

The test section is a 1.9 cm i.d. clear acrylic pipe, and is equipped with two fast-action pneumatic ball valves 200 cm apart. These two valves, which are normally open, are simultaneously activated and closed by a common compressed air valve, whereby the average gas hold-up in the test section is measured.

The lower mixer tank is a sealed transparent cylinder, with 13 cm i.d. and 13 cm height, and its top is fitted with a conical entrance to the test section, as shown in figure 2. Air is injected into the test section through a 5 cm long cylindrical distributor with 2 cm i.d, fitted with a porous stainless steel plate with 100 μm average pore diameter. The air supply line is fitted with needle valves, two rotameters, and a pressure gauge, which were utilized for adjusting and measuring the gas flow rate during the experiments.

The test section is connected to the top and bottom tanks via pipe fittings. For inclined channel experiments, bent tubes were added to the top and bottom of the test section. The configurations of the bends and fittings are shown in figure 3, and their dimensions are summarized in table 1.

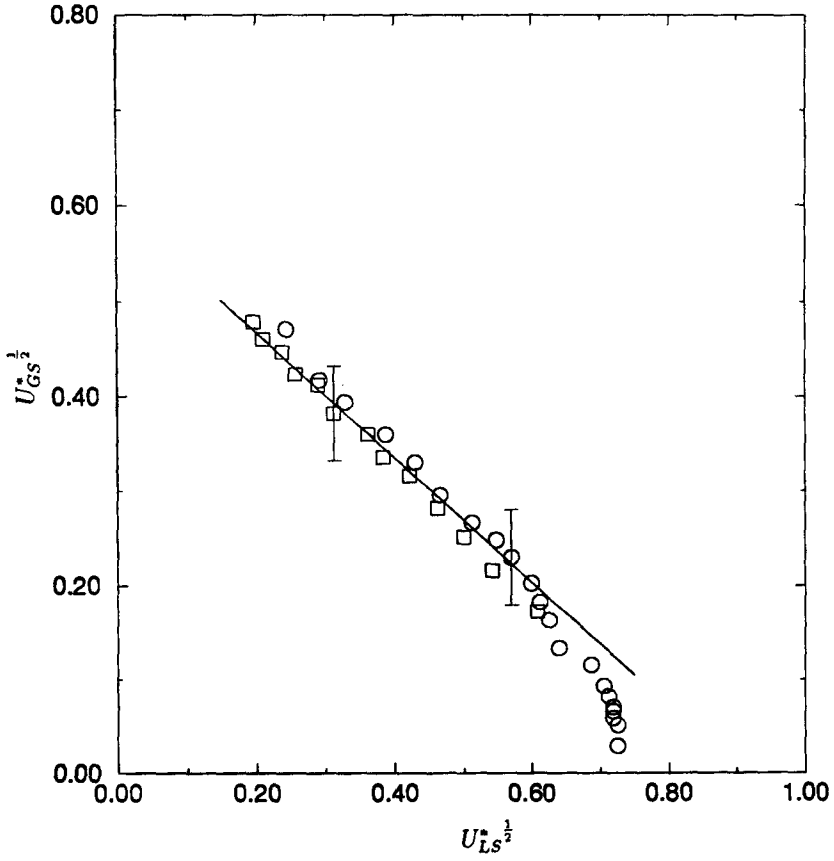

Figure 5. Flooding data for 30° channel angel of inclination: □, water; ○, mineral oil; —, flooding line [16], $m = 0.66$, $C = 0.6$.

Table 1. Bend fittings dimensions

Configuration	Length L_1 (cm)	Bend length (cm)	Bend radius of curvature (cm)
Vertical, $\theta = 0$, top	21	—	—
Vertical, $\theta = 0$, bottom	10	—	—
$\theta = 30°$, top	18	34	16
$\theta = 30°$, bottom	10	34	16
$\theta = 68°$, top	18	38	21
$\theta = 68°$, bottom	10	38	21

2.2. *Test procedure for flow regime and gas hold-up experiments*

At the start of each test, the lower mixing tank, the test section, and the overflow upper plenum were filled with liquid via injection at the top. Liquid continuously flowed through the system, with the flow rate controlled by the needle valve downstream of the mixer. The desired air flow rate was then set with the aforementioned needle valves and rotameters in the airline.

Following the establishment of a steady state in each test, the two-phase flow regimes in the test section were visually identified. The liquid flow rate was directly measured by the flowmeter downstream of the mixer and was confirmed by diverting the liquid to a graduated cylinder and measuring the amount collected over a period of several minutes. The pneumatic valves were then closed simultaneously, thereby trapping liquid and air in the test section and allowing the measurement of the gas hold-up (void fraction). The segment of the test section between the two quick-action valves was graduated, and was carefully calibrated to provide the test section average gas hold-ups corresponding to various collapsed liquid level locations, once the two valves were

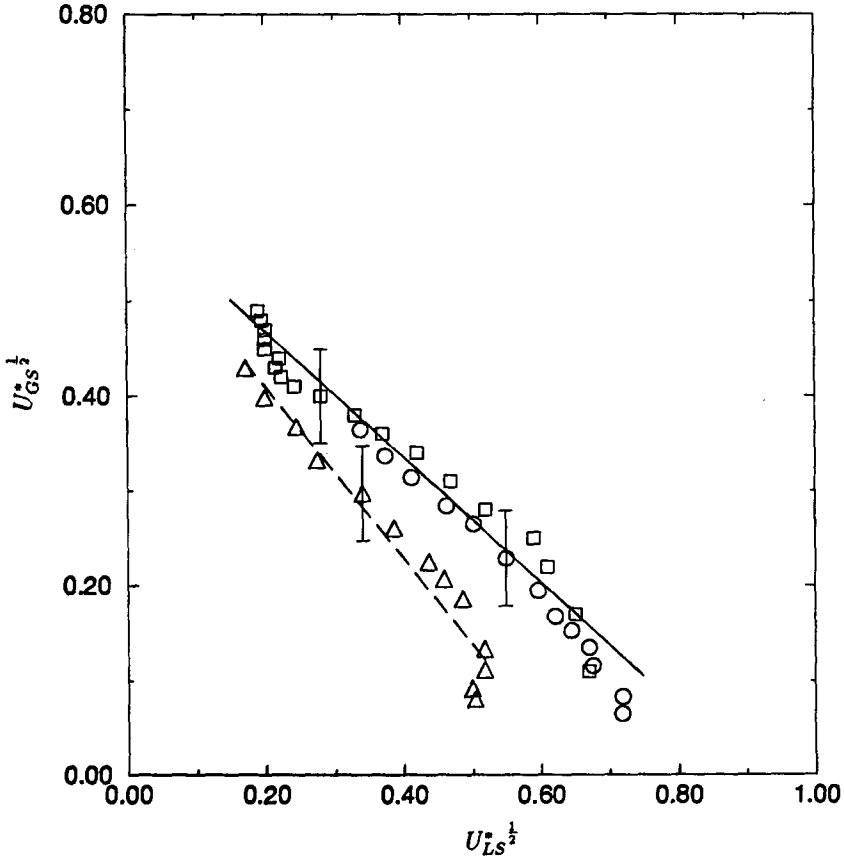

Figure 6. Flooding data for 60 and 68° channel angles of inclination, in tests with mineral oil: □, water (60°); ○, mineral oil (68°); △, paraffinic oil (68°); —, flooding line [16], $m = 0.66$, $C = 0.6$; – – –, flooding line [16], $m = 0.9$, $C = 0.6$.

closed. Calibration was done by filling the aforementioned segment of the test section, up to various levels and in all tested angles of inclination, with water, then draining and weighting the water.

Each of the gas hold-up measurement tests was repeated at least three times to examine repeatability and to account for data scatter characteristics. The typical scatter in measured gas hold-up resulting from the three times repetitions was ± 0.025.

2.3. *Test procedure for counter-current flow limitation (flooding) experiments*

At the start of each flooding test the pneumatic valves were closed and the upper plenum was filled with liquid. The liquid drain valve in the mixer tank was also closed. After opening the bleed valve in the mixer, the desired air flow rate was established. The pneumatic valves were then opened, and at the same time the bleed valve was closed and fluid flowed from the upper plenum, through the test section, filling the mixer tank. A steady state was established within a few seconds. A timer was started when the liquid level in the mixer tank reached a specific mark and stopped when a second mark was reached. The liquid superficial velocity in the test section was then calculated from the time required to fill the known volume between the two marked levels in the mixer. Each test was repeated at least three times and the results were averaged.

All tests were performed at room temperature in the 20–23°C range.

2.4. *Fluid properties*

Experiments were performed with demineralized water, a mineral oil, and a paraffinic oil. The relevant properties of the oils were directly measured. Neither of the oils contains polymeric molecules, and both behave as Newtonian fluids. Their measured properties are summarized in table 2, where properties of water at room temperature are also provided for comparison. The two oils have comparable surface tensions which are approximately five times smaller than water. Both the mineral and paraffinic oils are significantly more viscous than water, approximately by

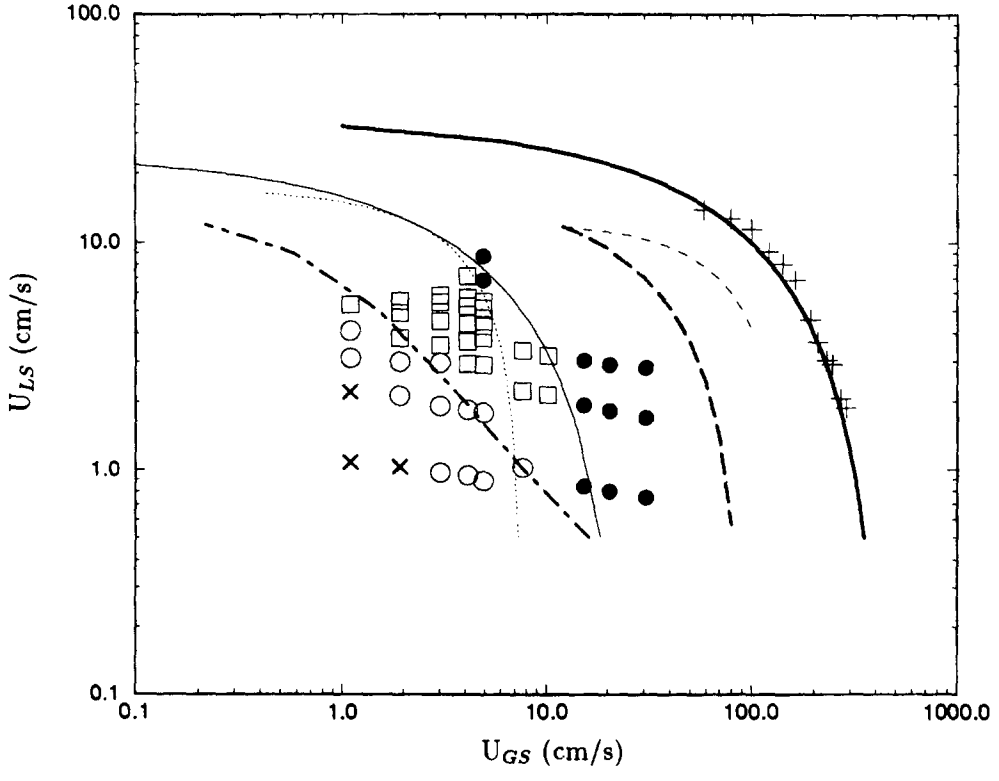

Figure 7. Air–water two-phase flow patterns for the vertical test section configuration: X, bubbly; ○, bubbly–slug/churn–slug; □, slug; ●, churn–annular; —, boundary b, Taitel and Barnea (1983), [1]; . . . ., boundary c, Taitel and Barnea (1983), [2]; +, CCFL; —, flooding line [16], $m = 0.66$, $C = 0.6$; – – – –, Usui (1989), [10]; - - - - -, Mishima and Ishii (1989) [4], with C_0 from [6], [7]; – – –, Mishima and Ishii (1989) [4], with $C_0 = 0.9$.

Table 2. Liquid properties at room temperature†

	Water	Mineral oil‡	Paraffinic oil§
Density (kg/m³)	996	843.1	871.4
Viscosity (Ns/m²)	1.00×10^{-3} at 20°	3.52×10^{-2} at 19.3°C	1.85×10^{-1} at 25°C
	0.789×10^{-3} at 30°C	2.28×10^{-2} at 27.5°C	0.982×10^{-1} at 38°C
Surface tension (N/m)	0.072	0.0136 at 26.5°C	0.0128
Property number, $Z = \left[\frac{\sigma^3 \rho_L}{g \mu_L^4}\right]^{1/3}$	3871	8.53 at 26.5°C	0.545
Viscosity number, $N_f = \frac{[D^3 g \rho_L \Delta\rho]^{1/2}}{\mu_L}$	9082	284.4 at 26.5°C	38.6

†At 25°C, unless otherwise stated.
‡Fisher Bath Oil, Fisher Scientific.
§R-620-13 Paraffinic Oil 3, Sun Oil Company.

factors of 35 and 185, respectively. The viscosities of the oils, furthermore, were found to be relatively sensitive to temperature.

2.5. *Experimental measurements and uncertainties*

The air flow rates were measured using two rotameters. At low air flow rates the rotameter used was Type R-225-B (Brooks Instruments), which had a range of 151–2217 cm³/min standard air with

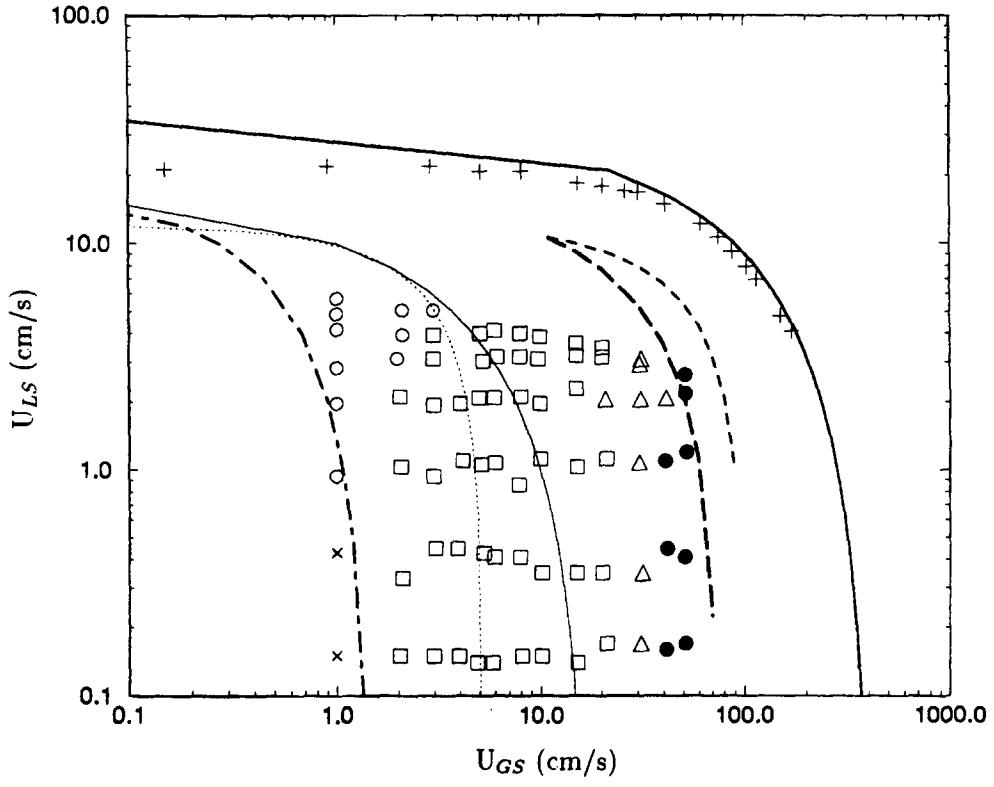

Figure 8. Air–mineral oil two-phase flow patterns for the vertical test configuration: X, bubbly; ○, bubbly/slug; □, slug; △, slug/froth; ●, froth; +, CCFL; —, boundary b, Taitel and Barnea (1983), [1]; . . . ., boundary c, Taitel and Barnea (1983), [2]; —, flooding line [16], $m = 0.66$, $C = 0.6$; – – – –, Usui (1989), [10]; - - - - - -, Mishima and Ishii (1989) [4], with C_0 from [6], [7]; – – –, Mishima and Ishii (1989) [4], with $C_0 = 0.9$.

glass ball, and 644–6655 cm³/min standard air with tantalum ball. Its accuracy was ±5% full scale, with a repeatability of 0.5% full scale. When the gas flow rate was beyond the capacity of the above rotameter, a Type R-615 B (Brooks Instruments) rotameter was used, which had a range of 390–23,870 cm³/min standard air, with an accuracy of ±5% full scale and a repeatability of 0.5% full scale.

In flooding tests the liquid flow rates were measured by collecting the liquid in a graduated 1000 cm³ cylinder, readable to within ±10 cm³, over periods of time measured with a stopwatch assumed to be accurate to within ±1 s. In tests dealing with flow patterns and gas hold-up, the liquid flow rate was measured using a Type R-8M-25-4F rotameter (Brooks Instruments) with a stainless steel ball. The accuracy of the rotameter was ±5% full scale, and its repeatability was 0.5% full scale. Its range, for mineral oil was 78–2567 cm³/min. The liquid temperature at the test section exit was measured using a calibrated mercury thermometer, with 0–100°C range and 0.1°C increments.

Uncertainties in the data can occur due to measurement errors. Based on the scale accuracy for liquid and gas flow meters, timer and pressure meters, uncertainties in measured gas and liquid superficial velocities are estimated as follows: uncertainty in U_{GS} is ±5%, and uncertainty in U_{LS} is ±8%. These, combined with a nominal 0.05 cm uncertainty in channel diameter, and a nominal 0.5°C variation in liquid temperature (which can affect surface tension and viscosity) resulted in the typical maximum uncertainty limits which will be depicted in the flooding data.

3. RESULTS AND DISCUSSIONS

Experiments were performed in this study with three test configurations: vertical, and inclined with respect to the vertical line by 30 and 68°, using water, and mineral and paraffinic oils. Most of the pure water data used here for comparison, were obtained in a previous study using

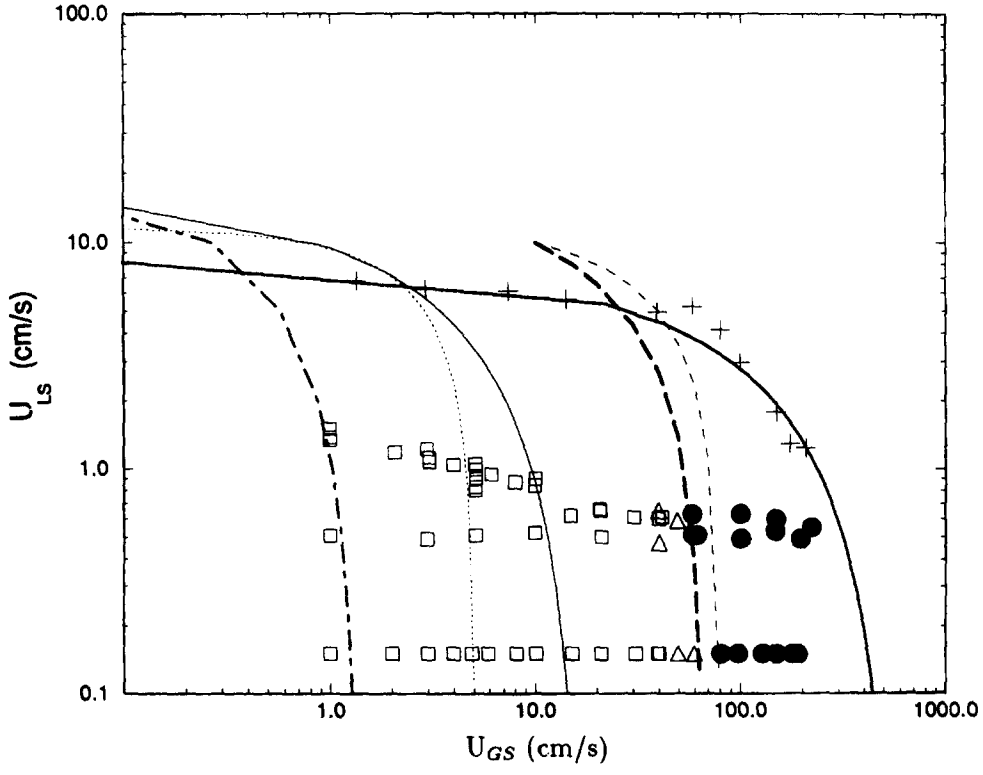

Figure 9. Air–paraffinic oil two-phase flow patterns for the vertical test section configuration: □, slug; △, slug/froth; ●, froth; +, CCFL; —, boundary b, Taitel and Barnea (1983), [1]; . . . ., boundary c, Taitel and Barnea (1983), [2]; —, flooding line [16], $m = 1.56$, $C = 0.692$; – – – –, Usui (1989), [10]; - - - - - -, Mishima and Ishii (1989) [4], with C_0 from [6], [7]; – – –, Mishima and Ishii (1989) [4], with $C_0 = 0.9$.

a similar test facility (Ghiaasiaan *et al.* 1995a), where the investigated configurations included vertical, and 28 and 60° angles of inclination. Flow regime, counter-current flow limitation, and gas hold-up data were generated in this study for all three configurations, with water and mineral oil. Fewer data were generated with paraffinic oil, however, since the oil had a foul odor and its vapor irritated the eyes. These included CCFL in vertical and 68°-inclined channels, and flow regime and gas hold-up experiments with the vertical channel configuration.

3.1. Counter-current flow limitation (CCFL)

The CCFL data are displayed in figures 4–6, where they are also curve-fitted using Wallis's flooding correlation, i.e. adjusting the parameters C and m to get the best fit between data and correlation (Wallis 1969)

$$U_{GS}^{*1/2} + mU_{LS}^{*1/2} = C, \qquad [16]$$

where m and C are generally constants of the order of 1. For simple vertical channels $m = 0.8$–1.0, and $C = 0.7$–1.0 have usually been reported, with C mainly depending on the channel end conditions (Bankoff and Lee 1986). Values for m and C significantly different than the aforementioned ranges have also been found for more complex channel configurations, however (Osakabe and Kawasaki 1989; Ohnuki 1986; Ghiaasiaan *et al.* 1995b). The dimensionless superficial velocities are defined as

$$U_{iS}^{*} = U_{iS}\left[\frac{\rho_i}{gD\Delta\rho}\right]^{1/2}, \quad i = \text{L or G}. \qquad [17]$$

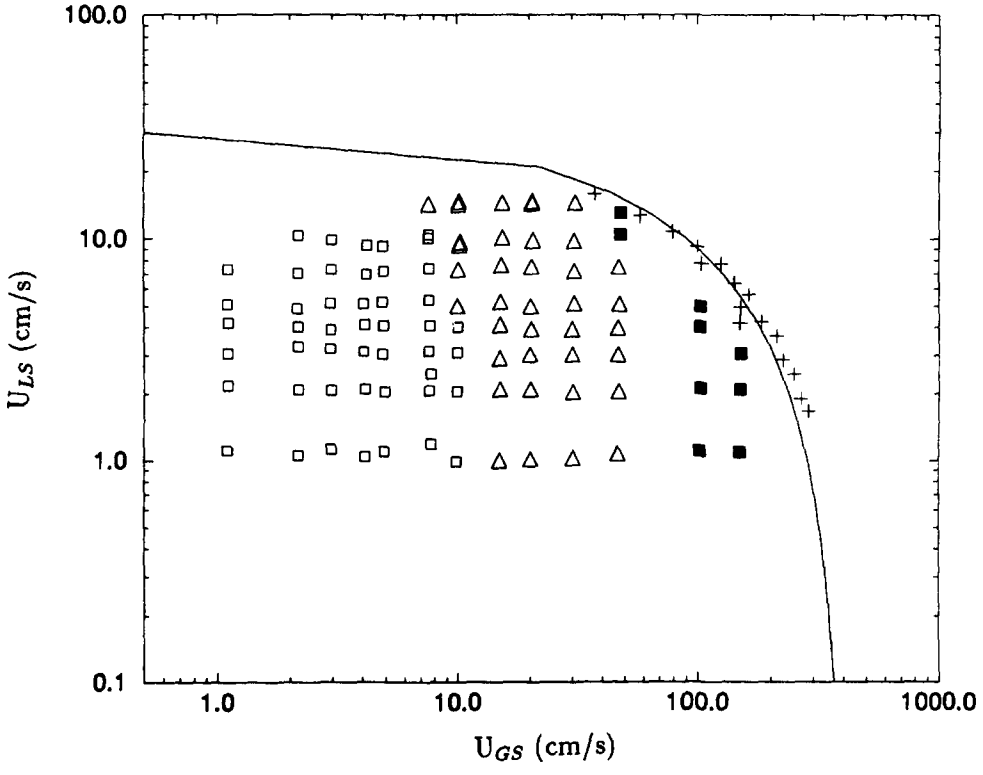

Figure 10. Air–water two phase flow patterns for 28° test section angle of inclination with respect to the vertical line: □, slug; △, churn–stratified; ■, semi-stratified; +, CFFL; —, flooding line [16], $m = 0.66$, $C = 0.6$.

Figure 4 depicts the CCFL data for the vertical channel configuration. The values of the inverse dimensionless viscosity, N_f (Wallis 1969), and the property number Z (Clift *et al.* 1966), defined in the forthcoming equations, are shown in table 2 for the three liquids

$$N_f = \frac{[D^3 g \Delta\rho \rho_L]^{1/2}}{\mu_L}, \quad [18]$$

$$Z = \left[\frac{\sigma^3 \rho_L}{g\mu_L^4}\right]^{1/3}. \quad [19]$$

Comparing the depicted data for demineralized water and the mineral oil in figure 4, it is noted that the reduction of Z and N_f by factors of 450 and 32, respectively, has no significant effect on the CCFL data, at least in the range $0.25 \leqslant U_{LS}^{*1/2} \leqslant 0.55$. In this range the CCFL data for water and mineral oil are well presented by Wallis's correlation [16], with $m = 0.66$ and $C = 0.6$, in agreement with the pure water data previously obtained with a similar test facility (Ghiaasiaan *et al.* 1995b). The effect of liquid properties on flooding have previously been studied by Clift *et al.* (1966) and Suzuki and Ueda (1977). Suzuki and Ueda examined the effects of both liquid viscosity and surface tension, and noticed that, with increasing the liquid viscosity the liquid film thickness at the onset of flooding increased. Furthermore, the effect of surface tension on their flooding data was complicated and, within their tested $0.038 \leqslant \sigma \leqslant 0.068$ N/m range, the gas superficial velocity at the onset of flooding appeared to maximized for $\sigma = 0.055$ N/m. Clift *et al.* (1966) measured only about 20% reduction in U_{GS}, for constant U_{LS}, when the liquid viscosity was increased by a factor of 70. These experimental studies, however, were both performed in test sections where liquid injection occurred through sintered segments of the test section. Experiments with the latter liquid injection arrangement are know to have flooding characteristics which are different than the characteristics of experiments in which liquid flows into the test channel from a partially-filled plenum (Ghiaasiaan *et al.* 1995b).

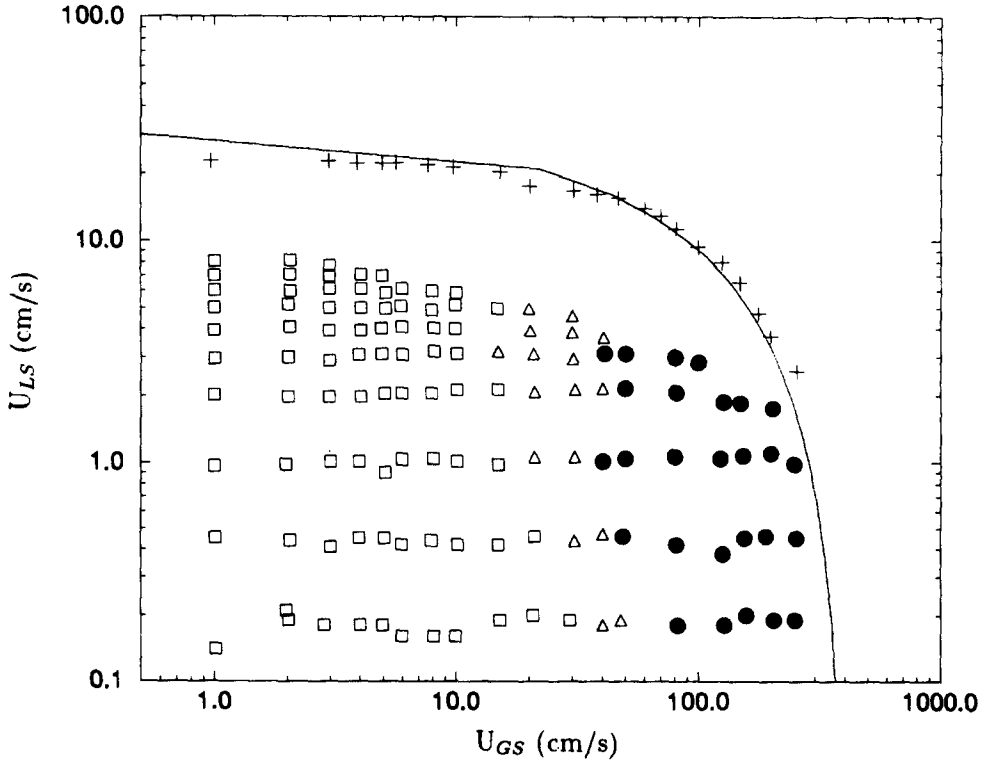

Figure 11. Air–mineral oil two phase flow patterns for 30° test section angle of inclination with respect to the vertical line: □, slug; △, churn/froth; ●, froth; +, CFFL; —, flooding line [16], $m = 0.66$, $C = 0.6$.

Demineralized water and mineral oil CCFL data obtained with 30 and 60° (water) and 68° (mineral oil) channel angles of inclination with the vertical line are also depicted in figures 5 and 6, respectively, and are noted to be similar, and follow Wallis's correlation with the aforementioned values of $m = 0.66$ and $C = 0.6$, independent of the test section angle of inclination, and in agreement with previous pure water experiments (Ghiaasiaan *et al.* 1995b). The mineral oil flooding data indicate slightly lower gas superficial velocities for the vertical channel and 68° angle of inclination (figures 4 and 6). An opposite trend is apparent in the data for the 30° angle of inclination (figure 5), however.

Figures 4 and 6 also display the CCFL data obtained with paraffinic oil. The property number Z for the latter fluid is of the order of 1 only, being smaller than Z for water and mineral oil by three and one orders of magnitude, respectively. The inverse dimensionless viscosity number, N_f, is also quite small for the tested paraffinic oil. Evidently, flooding characteristics of paraffinic oil are significantly different from either water or mineral oil. Furthermore, unlike water and mineral oil, the flooding curve for paraffinic oil is sensitive to the test section angle of inclination. For the vertical configuration the distribution of the latter data is in fair agreement with Wallis-type correlations, and the depicted best fit in figure 4 represents $m = 1.567$ and $C = 0.692$. With 60 and 68° angles of inclination (figure 6), on the other hand, deviation of the data from a linear distribution in the depicted coordinates is relatively significant at low U_{GS}, indicating rather poor compliance with Wallis-type correlations. The latter trend is also visible, to a lesser extent, in the water and mineral oil data for both 30 and 60–68° test section angles of inclination.

The apparent similarity of flooding curves representing water and mineral oil, and their difference with the flooding curves for the tested paraffinic oil, in figures 4–6, can be explained based on the dimensionless viscosity number, N_f. The latter parameter represents the ratio between buoyancy and viscous forces. In slug flow in vertical channels, $N_f > 300$ signifies a buoyancy (inertial)-dominated regime, while in the $N_f < 2$ range the process is viscosity-dominated (Wallis 1969). For counter-current flow limitation it may be reasonable to assume buoyancy-dominated flow when

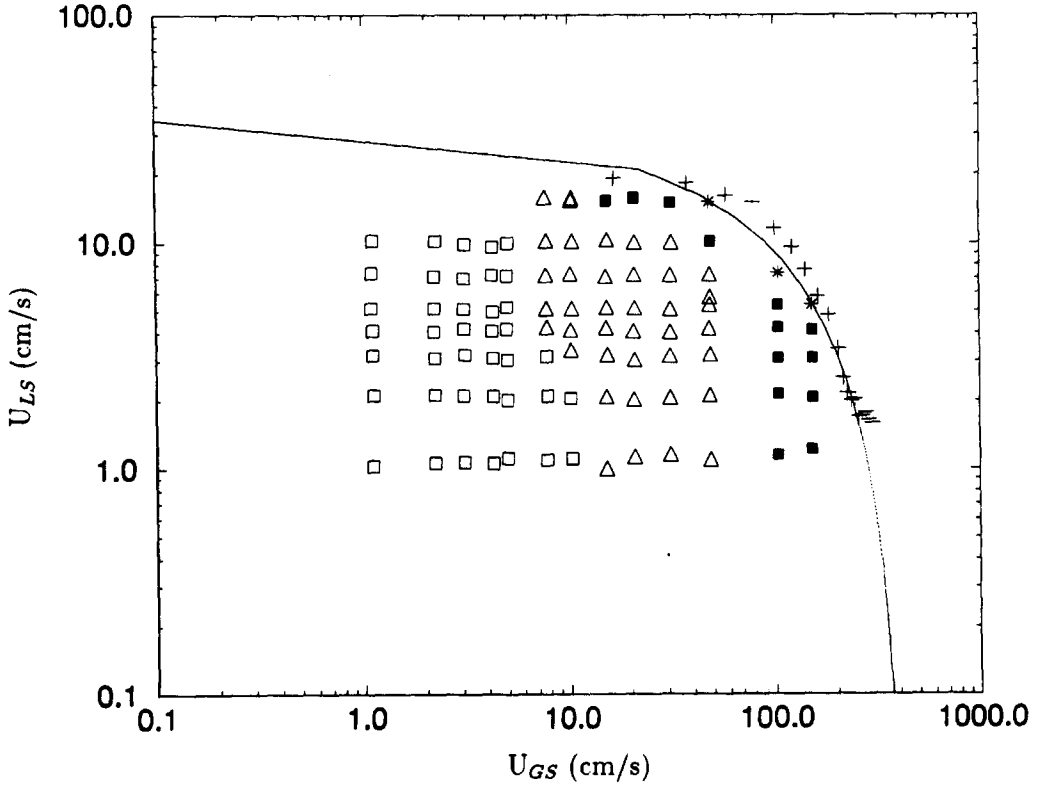

Figure 12. Air–water two phase flow patterns for 60° test section angle of inclination, with respect to the vertical line: □, slug; △, churn–stratified; ■, semi-stratified; +, CFFL; —, flooding line [16], $m = 0.66$, $C = 0.6$.

N_f is of the order 10^2 or larger. When buoyancy prevails, as is the case for water and other low viscosity liquids, flooding is relatively insensitive to changes in liquid viscosity. When $N_f \lesssim 10^2$, on the other hand, buoyancy and viscous forces are both significant, and liquid viscosity will affect flooding. In the latter case, the value of parameter m in Wallis's flooding correlation [16], is expected to increase as a result of increasing liquid viscosity, while parameter C (which mainly represents channel end geometric effects) should not change significantly. These observations are clearly supported by the data depicted in figures 4–6.

3.2. *Flow patterns*

The observed flow patterns in the vertical channel configuration are displayed in figures 7–9, for pure water, mineral oil, and paraffinic oil, respectively.

The major flow patterns with pure water (figure 7) included: (a) bubbly, represented by bubbles with little interactions; (b) bubbly-slug/churn-slug, where the bottom and top portions of the test section supported two different flow patterns with slug flow pattern at the top; (c) slug, represented by Taylor bubbles; and (d) churn–annular, where annular flow occurred over large segments of the channel, with intermittent flooding type waves forming at the test section bottom and moving upwards (Ghiaasiaan *et al.* 1995a). The models and correlations for flow pattern transitions reviewed in section 1 are also depicted in figure 7. The boundary b and boundary c models of Taitel and Barnea (1983) are in fair agreement with the data. The model of Usui (1989), represented by [10], underpredicts the gas superficial velocity for the establishment of churn flow at high liquid flow rates. The model of Mishima and Ishii (1984) [4] on the other hand, significantly disagrees with the data.

Figures 8 and 9 display the flow patterns in tests with mineral oil and the paraffinic oil, respectively, in the vertical channel configuration. In the flow pattern designated as bubbly/slug, the flow regime was predominantly bubbly, with short Taylor bubbles intermittently forming at the test section bottom. The froth flow pattern represented a chaotic regime with no discernible gas–liquid interphase configuration (Govier and Aziz 1972), and was therefore different from the

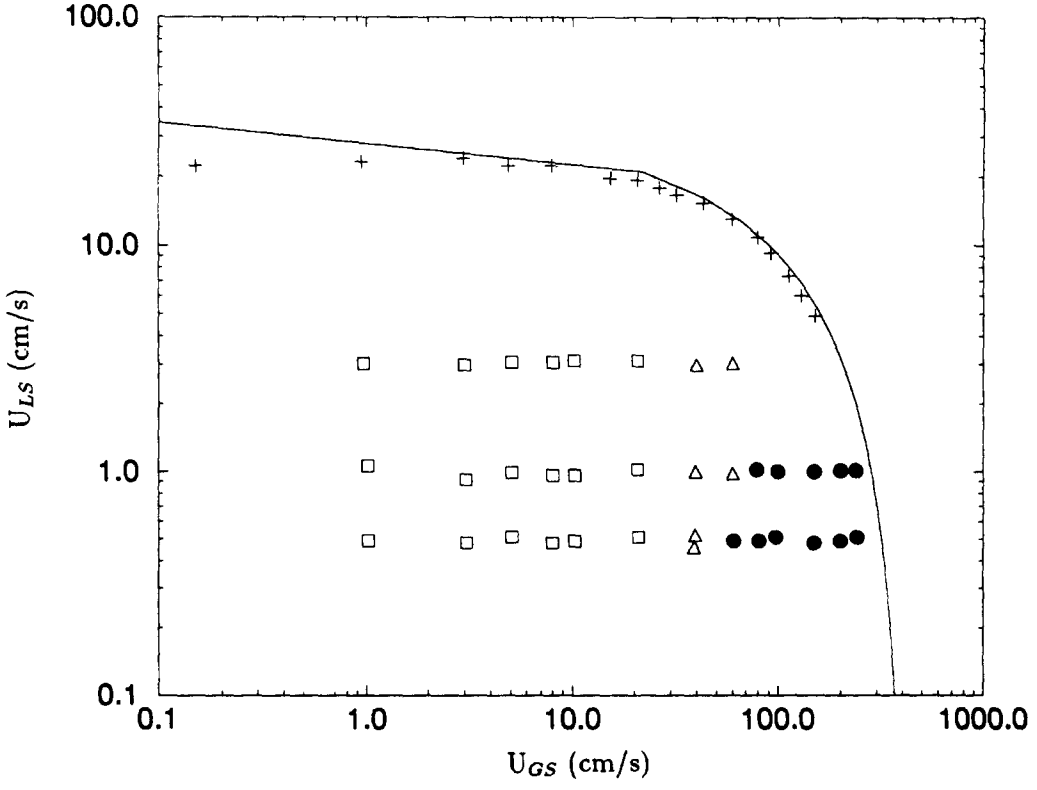

Figure 13. Air–mineral oil two phase flow patterns for 68° test section angle of inclination, with respect to the vertical line: □, slug; △, churn/froth; ●, froth; +, CFFL; —, flooding line [16], $m = 0.66$, $C = 0.6$.

churn flow pattern observed with pure water tests. The flow pattern designated as slug/froth was composed of Taylor bubble separated by relatively long regions of froth flow.

Comparison among figures 7–9 indicates that increasing liquid viscosity expands the parameter range in which the slug flow pattern is dominant. With water, within the liquid superficial velocity range covered in the tests, the slug flow pattern persisted as long as $U_{GS} \lesssim 13$ cm/s (see figure 7). With mineral and paraffinic oils, however, the slug flow pattern could be observed for $U_{GS} \lesssim 22$ and $\lesssim 40$ cm/s, respectively (see figures 8 and 9). The qualitative difference between churn flow pattern in pure water tests, and the froth flow pattern which replaces churn flow in tests with mineral and paraffinic oils should also be emphasized.

The aforementioned models for flow regime transitions are also depicted in figures 8 and 9, and are noted to significantly disagree with the data. An exception is the Mishima and Ishii (1984) model for slug to churn flow regime transition, which is in fair agreement with the paraffinic oil data displayed in figure 9.

Flow patterns are depicted in figure 10 for tests with pure water and 28° channel angle of inclination (Ghiaasiaan *et al.* 1995a), and in figure 11 for tests with the mineral oil and 30° angle of inclination. In figure 10, in the churn–stratified regime, the flow pattern in the channel was predominantly wavy stratified, periodically interrupted by upwards-moving flooding-type waves. In the semi-stratified flow regime the test section supported a periodic flow pattern where in each period the flow regime initially remained wavy stratified while liquid collected in the bottom portion of the test section and formed a large liquid slug which subsequently moved upwards in the channel. Stable stratified flow, however, did not occur. The latter flow pattern occurs only when a clear gas passway is possible (Weisman and Kang 1981), and therefore requires very large angles of inclination with respect to a vertical line (near horizontal). With mineral oil (figure 11), the slug flow pattern occurred over a considerably wider gas superficial velocity range and, more

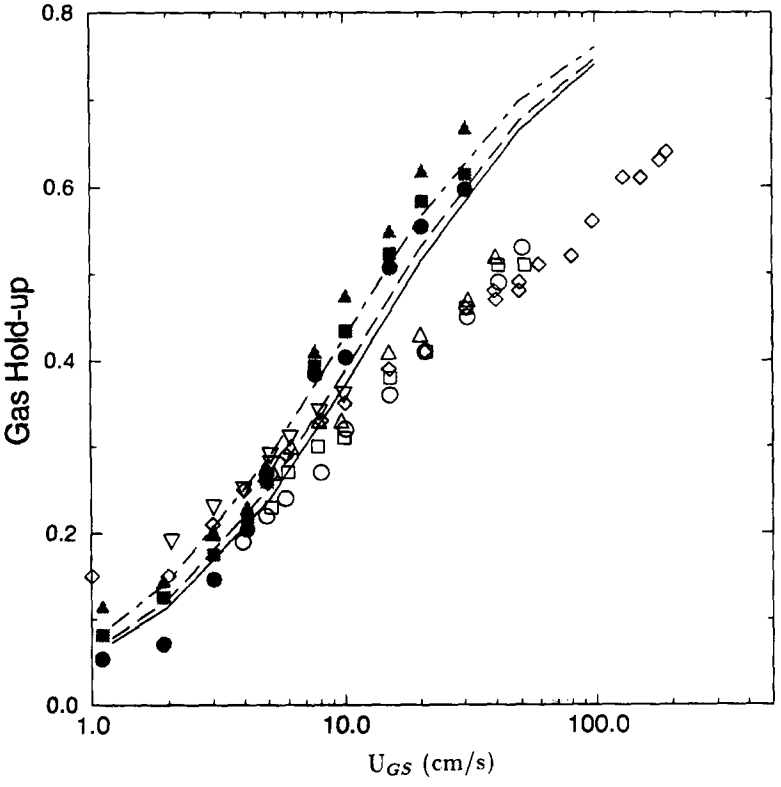

Figure 14. Gas hold-up in the vertical test section: parametric effects: ●, water, $U_{LS} = 0$; ■, water, $U_{LS} = 1$ cm/s; ▲, water, $U_{LS} = 3$ cm/s; ○, mineral oil, $U_{LS} = 0.15$ cm/s; □, mineral oil, $U_{LS} = 1$ cm/s; △, mineral oil, $U_{LS} = 3$ cm/s; ◇, paraffinic oil, $U_{LS} = 0$ cm/s; ▽, paraffinic oil, $U_{LS} = 1$ cm/s; —, Nicklin *et al.* (1962), [20], $U_{LS} = 0$; – – –, Nicklin *et al.* (1962), [20], $U_{LS} = 1$ cm/s; – – – – –, Nicklin *et al.* (1962), [20], $U_{LS} = 3$ cm/s.

importantly, churn-stratified and semi-stratified flow patterns were not observed at all, and were replaced with the aforementioned slug-froth and froth flow patterns. Furthermore, annular flow pattern was observed only in the aforementioned CCFL tests.

The churn-stratified and semi-stratified flow patterns also occurred in pure water tests with 60° channel angle of inclination (figure 12), and were absent in tests with mineral oil and 68° angle of inclination (figure 13), where, with increasing the gas superficial velocity the slug flow pattern gives way to the aforementioned froth flow. The latter flow pattern appears to persist up to close to the CCFL line, to be replaced with the annular flow pattern.

3.3. Gas hold-up

Figure 14 displays the measured channel average gas hold-ups (void fractions) for the vertical channel configuration. The measured pure water and mineral oil data include all the observed flow patterns of their respective fluids (see figures 7 and 8), except for annular flow pattern which occurred near CCFL conditions. With paraffinic oil, however, measurements were made only at $U_{LS} = 0$ and 1 cm/s, and all the data represent the slug flow pattern.

As noted in figure 14, the measured gas hold-ups for pure water are noticeably different from those representing either of the tested oils. For the $U_{GS} \leqslant 5$ cm/s range, where the flow regime in the depicted $U_{LS} \leqslant 3$ cm/s range was mainly bubbly in pure water (figure 7) and slug for both oils (figures 8 and 9), pure water experiments generally show the expected smaller gas hold-ups. In the $U_{GS} \geqslant 5$ cm/s range, however, the measured gas hold-ups are considerably lower for both oils, likely due to lower bubble rise velocities in them.

Figure 14 also depicts the predictions of the following correlation (Nicklin *et al.* 1962)

$$\alpha = \frac{U_{GS}}{C_0(U_{GS} - U_{LS}) + U_{B,\infty}}, \qquad [20]$$

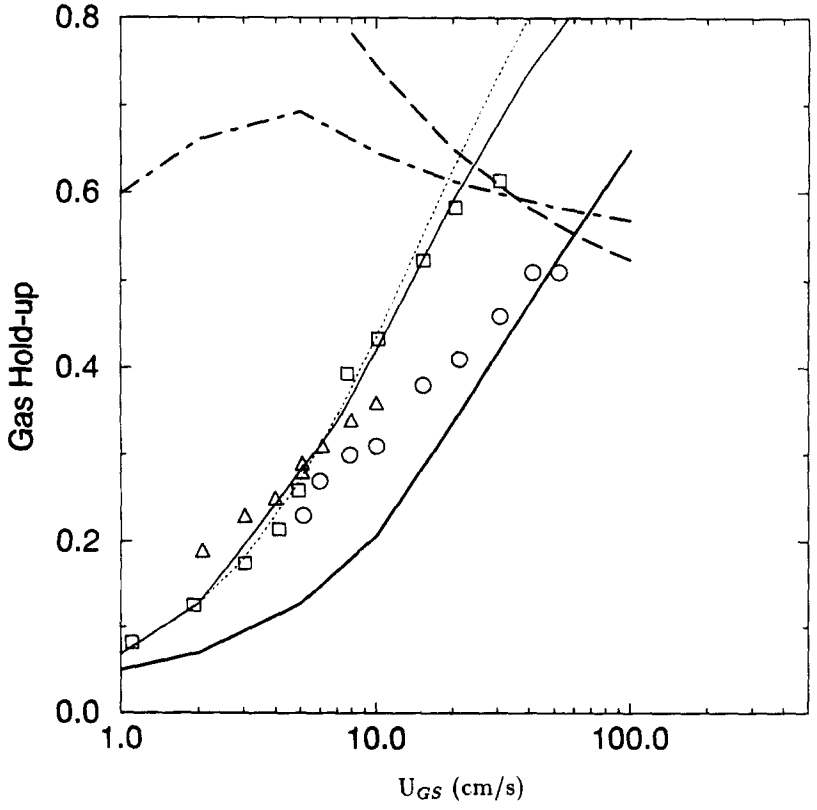

Figure 15. Gas hold-up in the vertical test section: comparison with two empirical correlations: □, water; ○, mineral oil; △, paraffinic oil; —, Usui (1989), water; . . . ., Usui (1989), mineral oil and paraffinic oil; —, Yamaguchi and Yamazaki (1982), water; - - - - -, Yamaguchi and Yamazaki (1982), mineral oil; – – –, Yamaguchi and Yamazaki (1982), paraffinic oil.

where $U_{B,\infty}$ representing the rise velocity of Taylor bubbles, is found from [14] with $C_1 = 0.35$ (Davidson and Harrison 1971). The latter correlation, which well-predicts the counter-current gas hold-ups for water in slug and churn flow patterns (Ghiaasiaan *et al.* 1995a), is evidently in poor agreement with the data representing either of the tested oils, due to the significance of liquid viscosity in the latter liquids.

The existing empirical correlations for gas hold-up are generally based on experimental data obtained with water and other low viscosity liquids, and are mostly inappropriate for liquid viscosities significantly different than water. Figure 15, for example, compares a set of our data with the predictions of the drift flux model [5], [9], where C_0 and V_{Gj} are calculated based on the recommendations of Usui (1989), [12]–[15], where $V_{Gj} = U_{B,\infty}$. Figure 15 also compares the predictions of the empirical correlation of Yamaguchi and Yamazaki (1982), which explicitly includes the liquid viscosity, with the experimental data. Both correlations evidently are inappropriate for the tested high viscosity liquids.

The pure water, mineral and paraffinic oil data, when curve-fitted to the drift flux model [5], [9], where $V_{Gj} = U_{B,\infty}$ is assumed and the latter is found from [14], are depicted in figure 16. As noted, for total volumetric fluxes in the range $U_m \geqslant 2$ cm/s, for each of the liquids all the data correlate with a single set of C_0 and C_1 values reasonably well. These parameters, however, appear to be strong functions of liquid viscosity and surface tension. Our measured data are evidently insufficient for the development of a general correlation. Experiments aimed at generation of more data, and providing for the development of reasonably general correlations for C_0 and C_1 are recommended.

The gas hold-up data measured in tests with inclined channels are now discussed.

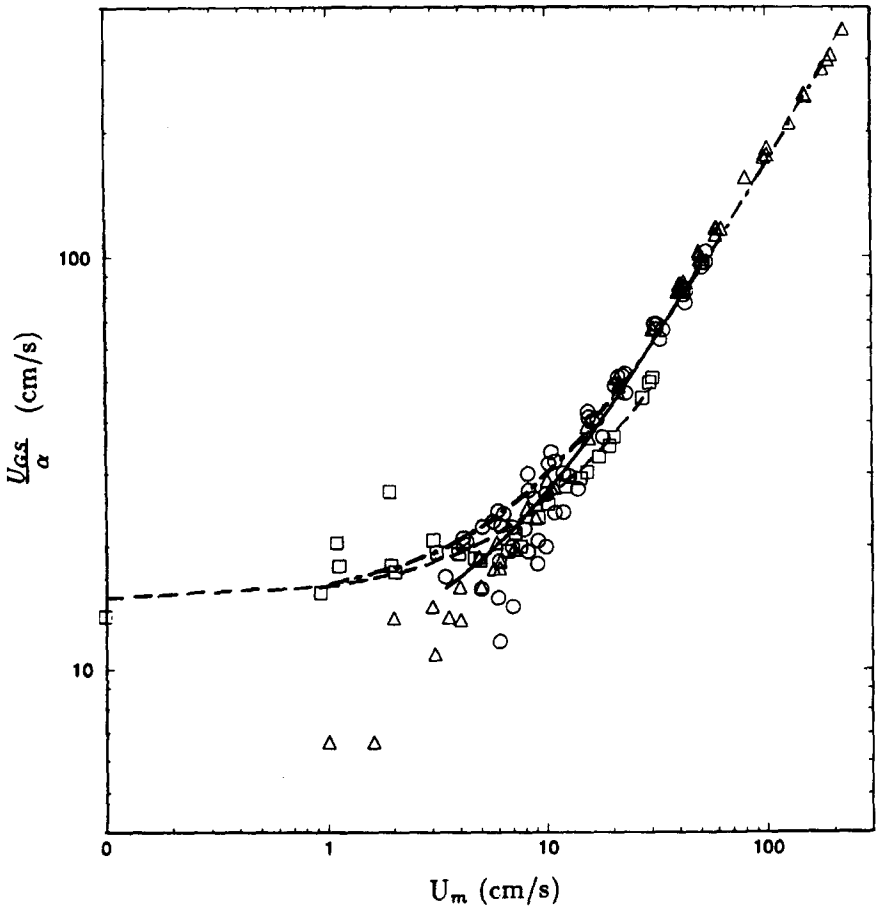

Figure 16. Drift flux model parameters adjusted for the vertical test section gas hold-up data: □, water; – – –, water, $C_0 = 1.2$, $C_1 = 0.35$; ○, mineral oil; —, mineral oil, $C_0 = 1.7$, $C_1 = 0.23$; △, paraffinic oil; – – – – –, paraffinic oil, $C_0 = 1.55$, $C_1 = 0.34$.

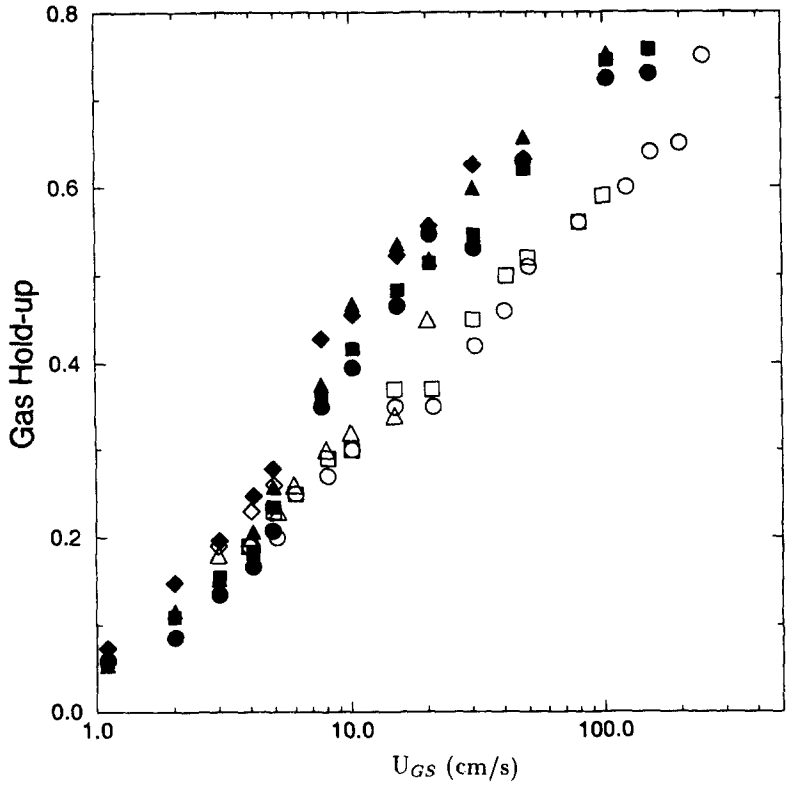

Figure 17. Gas hold-up for 28 and 30° channel angles of inclination: ●, water, 28°, U_{LS} = 1 cm/s; ○, mineral oil, 30°, U_{LS} = 1 cm/s; ■, water, 28°, U_{LS} = 3 cm/s; □, mineral oil, 30°, U_{LS} = 3 cm/s; ▲, water, 28°, U_{LS} = 5 cm/s; △, mineral oil, 30°, U_{LS} = 5 cm/s; ◆, Water, 28°, U_{LS} = 7 cm/s; ◇, mineral oil, 30°, U_{LS} = 7 cm/s.

Figures 17 and 18 display the gas hold-up data representing the 28–30° and 60–68° inclined test sections, respectively. For these inclined configurations the gas hold-up measurements were only performed for water and mineral oil. As noted in both figures, the gas hold-up distributions, while being relatively insensitive to U_{LS}, are different for the two fluids, in particular in the $U_{GS} \geqslant 5$ cm/s range. Comparison among data obtained with the same liquid and at different angles of inclination, typified by figure 19, shows the relative insensitivity of gas hold-up to the angle of inclination. The small difference between the gas hold-ups in the slug flow pattern, furthermore are consistent with the previously reported effect of channel angle of inclination on the terminal velocity of Taylor bubbles in low viscosity liquids. Zukoski (1966) experimentally studied the propagation velocity of Taylor bubbles in vertical and inclined channels. For low viscosity liquids, and over a wide range of surface tensions and channel diameters, the propagation velocity of Taylor bubbles increased as the angle of inclination with respect to the vertical line was increased from zero to almost 45°; and the trend reversed thereafter, and further increase in the angle of inclination resulted in a reduction of the bubble velocity. Since higher Taylor bubble velocity reduces the channel gas hold-up, the channel gas hold-up in slug flow should also decrease as the angle of inclination is increased from zero to 45°, and should increase afterwards. These trends were observed in our tests with inclined channels, for water as well as the tested mineral oil.

4. CONCLUDING REMARKS

Two-phase flow patterns, counter-current flow limitation (flooding), and gas hold-up associated with counter-current flow in channels with 0, 28–30° and 60–68° angles of inclination with respect to the vertical line were experimentally studied in a 2 m-long test section with 1.9 cm inner diameter. Near-atmospheric air at room temperature was the gas phase, and deionized water, a mineral oil (0.0136 N/m surface tension at 26.5°C, 3.52×10^{-2} Ns/m^2 viscosity at 19.3°C), and

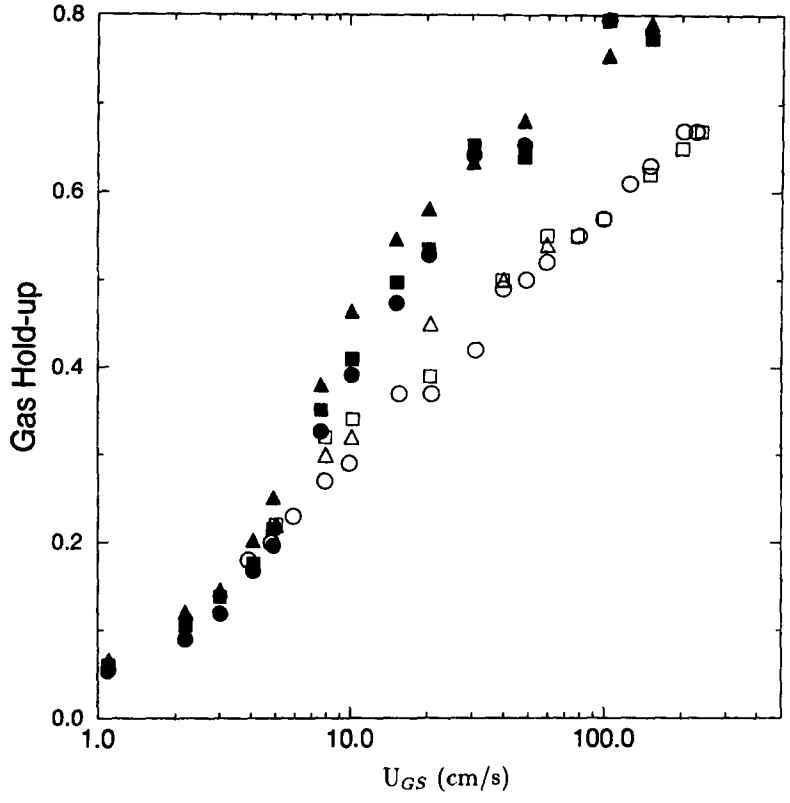

Figure 18. Gas hold-up for 60 and 68° test section angle of inclination: ●, water, 60°, $U_{LS} = 0$; ○, mineral oil, 68°, $U_{LS} = 0$; ■, water, 60°, $U_{LS} = 1$ cm/s; □, mineral oil, 68°, $U_{LS} = 1$ cm/s; ▲, water, 60°, $U_{LS} = 3$ cm/s; △, mineral oil, 68°, $U_{LS} = 3$ cm/s.

a paraffinic oil (0.0128 N/m surface tension and 1.85×10^{-1} Ns/m^2 viscosity at 25°C) were used as the liquid phase. The liquid and gas superficial velocity ranges were as follows: for tests with pure (demineralized) water $0 \leqslant U_{LS} \leqslant 54$ *cm/s and* $1 \leqslant U_{GS} \leqslant 299$ cm/s, respectively; for tests with mineral oil $0 \leqslant U_{LS} \leqslant 23$ cm/s and $1 \leqslant U_{GS} \leqslant 248$ cm/s, respectively, and for tests with paraffinic oil $0.15 \leqslant U_{LS} \leqslant 11.6$ cm/s and $1 \leqslant U_{GS} \leqslant 224$ cm/s, respectively.

The major flow patterns with water were bubbly, slug, churn, and churn–annular in the vertical configuration, and slug, churn–stratified and semi-stratified in inclined channels. With the tested oils, however, slug, slug–froth and froth were the dominant flow patterns with all angles of inclination. The measured void fractions were also different for the oils than water, and were generally lower in the superficial velocity ranges associated with the slug and froth flow patterns.

Several existing models and correlations dealing with conditions under which the slug flow pattern is disrupted were compared with the data, generally with poor agreement. Some existing correlations for void fraction were also examined, and were found to disagree with the data obtained with the oils.

The flooding data for water and the mineral oil were similar, and were insensitive to the angle of inclination. The flooding curve for the paraffinic oil was considerably lower than water, however, and varied with the angle of inclination.

Based on the results obtained in this study, the following are recommended:

(1) more systematic experiments aimed at better understanding the effects of liquid properties on flow patterns are needed;

(2) more void fraction data are needed for the development of correlations for the two-phase drift flux distribution coefficient, C_0, and gas drift velocity, applicable to highly viscous liquids.

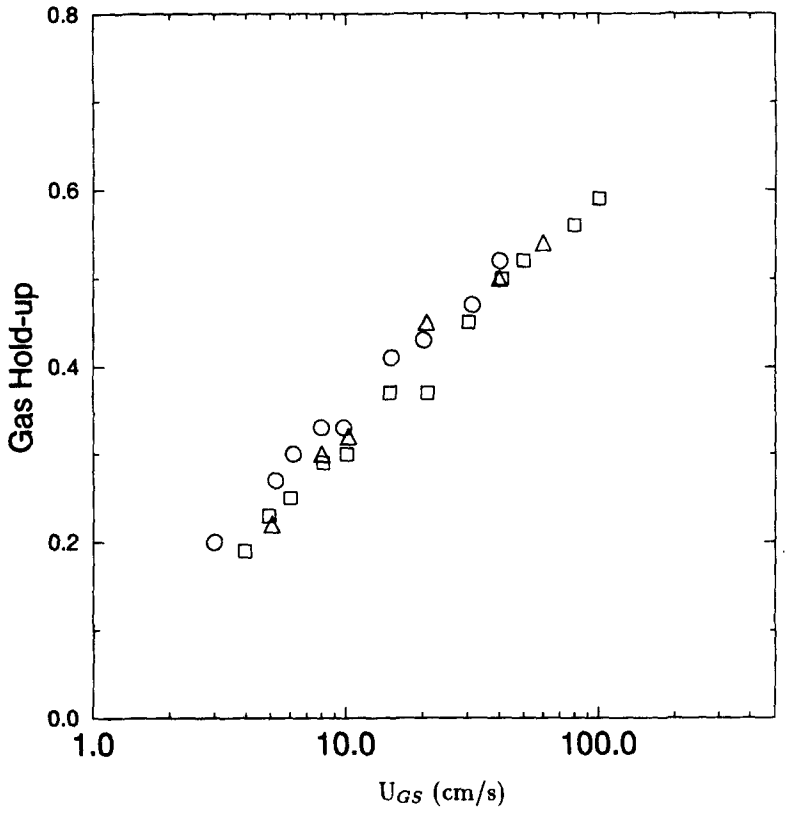

Figure 19. The effect of test section angle of inclination on the gas hold-up, in tests with mineral oil: ○, vertical channel; □, 30° inclined channel; △, 68° inclined channel.

REFERENCES

Amarasooriya, W. H. and Theofanous, T. G. (1988) Premixing of steam explosions: a three-fluid model. *Proc. 25th ASME–AIChE National Heat Transfer Conference*, Houston, Texas, July 1988, pp. 191–200.

Bankoff, S. G. and Lee, S. C. (1986) A critical review of the flooding literature. In *Multiphase Science and Technology*, ed. G. F. Hewitt, J. M. Delhaye and N. Zuber, Vol. 2, pp. 95–180. Hemisphere, New York.

Brauner, N. and Barnea, D. (1986) Slug/churn transition in upward gas–liquid flow. *Chem. Engng Sci.* **41,** 159–163.

Carlson, K. E. *et al.* (1990) RELAP5/MOD3 code manual, Volumes 1, 2, 3, NUREG/CR-5535, US Nuclear Regulatory Commission.

Clift, R., Pritchard, C. L. and Nedderman, R. M. (1966) The effect of viscosity on the flooding conditions in wetted wall columns. *Chem. Engng Sci.* **21,** 87–95.

Davidson, J. F. and Harrison, D. (1971) *Fluidization*. Academic Press, New York.

Ghiaasiaan, S. M., Taylor, K. E., Kamboj, B. K. and Abdel-Khalik, S. I. (1995a) Countercurrent two-phase flow regimes and void fraction in vertical and inclined channels. *Nuclear Sci. Engng* **119,** 182–194.

Ghiaasiaan, S. M., Turk, R. E. and Abdel-Khalik, S. I. (1995b) Countercurrent flow limitation in inclined channels with bends. *Nucl. Engng Des.* **152,** 379–388.

Govier, G. W. and Aziz, K. (1972) *The Flow of Complex Mixtures in Pipes*. Robert E. Krieger Publishing Company, Malabar, FL.

Harmathy, T. Z. (1960) Velocity of large drops and bubbles in media of infinite or restricted extend. *AIChE J.* **6,** 281–288.

Jayanti, S. and Hewitt, G. F. (1992) Prediction of the slug-to-churn flow transition in vertical two-phase flow. *Int. J. Multiphase Flow* **18,** 847–860.

Martin, C. S. (1976) Vertically downward two-phase slug flow. *J. Fluids Eng.* **98,** 715–722.
McQuillan, K. W. and Whalley, P. B. (1985) Flow patterns in vertical two-phase flow. *Int. J. Multiphase Flow* **11,** 161–175.
Mishima, K. and Ishii, I. (1984) Flow regime transition criteria for two-phase flow in vertical tubes. *Int. J. Heat Mass Transfer* **27,** 723–734.
Nicklin, D. J., Wilkes, J. O. and Wilkes, J. F. (1962) Two-phase flow in vertical tubes. *Trans. Inst. Chem. Engrs* **40,** 61.
Ohnuki, A. (1986) Experimental study of counter-current two-phase flow in horizontal tube connected to inclined riser. *J. Nucl. Sci. Technol.* **23,** 219–232.
Osakabi, M. and Kawasaki, Y. (1989) Top flooding in thin rectangular and annular passages. *Int. J. Multiphase Flow* **15,** 747–754.
Passamehmetoglu, K. O. *et al.* (1990) TRAC-PF1/MOD2 Theory manual. Draft Report, Los Alamos National Laboratory, Los Alamos, NM.
Ren, W. M., Ghiaasiaan, S. M. and Abdel-Khalik, S. I. (1994) GT3F: an implicit finite-difference computer code for transient three-dimensional three-phase flow. Part I: governing equations and solution scheme. *Num. Heat Transfer, Part B: Fundamentals* **25,** 1–20.
Suzuki, S. and Ueda, T. (1977) Behavior of liquid films and flooding in counter-current two-phase flow—Part I. Flow in circular tubes. *Int. J. Multiphase Flow* **3,** 517–532.
Taitel, Y. and Barnea, D. (1983) Countercurrent gas–liquid vertical flow, model for flow pattern and pressure drop. *Int. J. Multiphase Flow* **9,** 637–647.
Usui, K. (1989) Vertically downward two-phase flow, (II) flow regime transition criteria. *J. Nucl. Sci. Technol.* **26,** 1013–1022.
Wallis, G. B. (1969) *One Dimensional Two-phase Flow.* McGraw-Hill, New York.
Weisman, J. and Kang, S. Y. (1981) Flow pattern transitions in vertical and upwardly inclined lines. *Int. J. Multiphase Flow* **7,** 271–291.
Yamaguchi, K. and Yamazaki, Y. (1982) Characteristics of countercurrent gas–liquid two-phase flow in vertical tubes. *J. Nucl. Sci. Technol.* **19,** 985–996.
Yamaguchi, K. and Yamazaki, K. (1984) Combinated flow pattern map for cocurrent and countercurrent air–water flows in vertical tubes. *J. Nucl. Sci. Technol.* **21,** 321–327.
Zukoski, E. E. (1966) influence of viscosity, surface tension, and inclination angle on motion of long bubbles in closed tubes. *J. Fluid Mech.* **25,** 821–837.